SCIENCE CHINA
Information Sciences

August 2019, Vol. 62 080302:1–080302:13
https://doi.org/10.1007/s11432-018-9837-9

• RESEARCH PAPER •
Special Focus on B5G Wireless Communication Networks

Analysis of irregular repetition spatially-coupled slotted ALOHA

Hanxiao YU[1], Zesong FEI[1*], Congzhe CAO[2], Ming XIAO[3], Dai JIA[1] & Neng YE[1]

[1]*School of Information and Electronics, Beijing Institute of Technology, Beijing* 100081*, China;*
[2]*Department of Electrical and Computer Engineering, University of Alberta, Edmonton* AB T6G 1H9*, Canada;*
[3]*School of Electrical Engineering, KTH Royal Institute of Technology, Stockholm* 100 44*, Sweden*

Received 5 November 2018/Revised 5 January 2019/Accepted 13 March 2019/Published online 11 July 2019

Abstract Contention-based access is a promising technology for massive and sporadic transmissions. In this paper, we propose a novel contention-based multiple access scheme, named irregular repetition spatially-coupled slotted ALOHA (IRSC-SA), motivated by the spatial coupling and irregular repetition techniques. There are different classes of users and slots in IRSC-SA, which result in unequal protection for different users. Considering that, we derive a novel density evolution (DE) method, which deals with unequal packet protection and introduces Bayesian reasoning to analyze the throughput threshold of the proposed IRSC-SA. Theoretical analysis and simulation results show that the proposed scheme achieves better asymptotic threshold and system packet throughput performance than the conventional spatially-coupled slotted ALOHA.

Keywords spatial coupling, coded slotted ALOHA, contention-based access, density evolution, irregular repetition

Citation Yu H X, Fei Z S, Cao C Z, et al. Analysis of irregular repetition spatially-coupled slotted ALOHA. Sci China Inf Sci, 2019, 62(8): 080302, https://doi.org/10.1007/s11432-018-9837-9

1 Introduction

The fifth generation (5G) wireless communication systems are evolving rapidly, where massive machine type of communications (mMTC) is a key promise that enables seamlessly connections of a variety of smart devices and aims at providing inter-connections among large number of devices [1,2]. As the 5G systems are being launched for commercial uses and studies on the beyond 5G (B5G) systems have been carried out actively, the number of connected devices foresees even more tremendous increases. In the vision of B5G systems, hundreds of millions of vehicle-mounted communication devices are to be found across land, sea and sky [3]. A huge amount of intelligent sensors will be deployed throughout a wide variety of natural environment and even planted in living organisms [4]. In order to investigate the quality of wireless access services for these communication devices, some new communication paradigm are considered for B5G systems, such as ultra-dense heterogenous networks and space-based backbone networks. The new arising scenarios for B5G systems require rigorous demands such as high spectral efficiency, intelligence transmissions, high reliability, low latency and endogenous security, where a large amount of users with small packages produce unpredictable activation patterns. Therefore, the B5G communications impose significant challenges on the current wireless access techniques. To address the challenge of massive connectivity, new techniques for multiple access in physical (PHY) and medium access control (MAC) layer have been investigated [5]. Physical layer non-orthogonal multiple access

* Corresponding author (email: feizesong@bit.edu.cn)

(NoMA) scheme is a promising multi-access method for B5G which superposes messages from multiple users within the same resource block in either power domain or code domain [6].

Most of typical NoMA schemes, such as power-domain non-orthogonal multiple access (PD-NOMA) [6], multi-user shared access (MUSA) [7], and sparse code multiple access (SCMA) [8], rely on careful scheduling at the network side, which results in large signaling overhead and high latency [9]. On the other hand, B5G networks are expected to provide superior performance in latency, reliability and connectivity than those of legacy systems. Considering the the visions and challenges for B5G systems, the random access technologies are agile and flexible to provide wireless connectivity for mobile devices, which is worth to be further exploited to meet the stringent demands. Modern random access reduces signaling overhead and transmission delay, and is emerging as an efficient yet simple solution for arising Internet of things (IoT) applications in upcoming beyond-5G systems. In particular, contention-based multiple access is proposed as a MAC-layer solution, where the scheduling procedures between devices and the network side are omitted to reduce the signaling overhead and latency. Contention-based MUSA and SCMA have been proposed, where once devices have data in buffer, they transmit the signals according to randomly selected spreading signatures [7, 10].

Another class of promising contention-based access technologies which exploit the reciprocity between coding and slotted ALOHA (SA) has been investigated over the past years [11–18]. With the simple form, SA schemes are more suitable to be applied in the low-cost and low-complexity devices for B5G systems. Ref. [11] proposes a grant-free rateless multiple access scheme, where the transmitter is considered as linear superposition of the rateless encoders [19–21]. Ref. [12] proposes a multiple access analog fountain coding scheme, and applies iterative decoding to recover source information. Several graph-based SA schemes have been proposed for different application scenarios, where the packet transmission and recovery is represented by a Tanner graph [14–17, 22–25].

The diversity slotted ALOHA (DSA) scheme generates multiple replicas of one message within a frame to achieve the diversity gain [13]. Based on DSA, the authors in [14] proposed collision-resolution diversity slotted ALOHA (CRDSA) which benefits from a fixed number of repetition of the bursts and inter-slot successive interference cancelation (SIC) detection. In CRDSA, SIC is applied at the receiver to overcome collisions among different users and provide significant performance improvement with respect to DSA. Then it is shown in [15] that, better performance can be achieved in binary erasure channels with irregular-repetition slotted ALOHA (IRSA) where the burst repetition is a variable and is optimally designed with a bipartite graph. In [16], a further generalization of IRSA called coded slotted ALOHA (CSA) is proposed where the packets are encoded with linear block codes [26–28] instead of transmitting replicas and SIC is combined with linear block code decoding to recover source packets.

Since the number of repetitions of a burst is usually much smaller than the length of frame, the corresponding Tanner graph of graph-based CSA is sparse, and the graph representation is similar to the Tanner graph as used in low density parity check (LDPC) codes [17]. Hence, the theory of codes on graphs can be applied to optimize access schemes. Therefore, the theory and tools from codes-on-graphs like density evolution (DE), as having been used to track the probabilities in the decoding process of LDPC codes, can be utilized to model the decoding process of graphical-based SA [15–17, 22, 23, 25].

Recent study on LDPC codes shows that improved iterative decoding thresholds can be achieved with spatial coupling [29]. The original structure of the spatially-coupled models goes back to the convolutional LDPC code proposed in 1999 [30]. Spatial coupling has emerged as a useful tool in the design and analysis of graphical models. Basic LDPC ensembles are coupled together to conduct a chain, and the neighboring ensembles are connected by a set of edges. Iterative decoding progresses through the spatially coupled (SC) chain starting from each end. Based on this observation, Ref. [31] proposes spatially-coupled slotted ALOHA (SC-SA) by integrating spatial coupling with SA. Considering that the iterative decoding thresholds of irregular LDPC codes more closely approach the Shannon limit compared with their regular counterparts [32], we propose an irregular repetition spatially-coupled slotted ALOHA (IRSC-SA) scheme, which applies the theory of irregular repetition in spatially-coupled slotted ALOHA. In conventional graph-based SA schemes, all users share the same access behavior and all slots are equally accessible. It is noted that in conventional graph-based SA schemes, all users are equally protected statistically

while the average overload of each slot may differ due to spatial coupling in IRSC-SA, hence packets transmitted by various users have different recovery probabilities. Therefore, the arithmetic average of the erasure probabilities, which has been adopted in the conventional DE [15, 18, 22–25, 31], cannot accurately describe the erasure probability when spatial coupling is incorporated in SA. Based on the unique design of IRSC-SA, we modified the original DE by taking consideration of different types of SNs and BNs. Specially, our main contributions can be outlined as follows:

(i) The irregular repetition spatially-coupled slotted ALOHA (IRSC-SA) scheme is proposed, which is shown to achieve significant throughput gain with integration of spatial coupling and irregular repetition. Then, we describe the scheme with Tanner graph, where the users and slots are represented by burst nodes (BNs) and slot nodes (SNs), respectively.

(ii) Considering that SNs and BNs are treated equivalently in terms of packet erasure probability and BNs have different error protection in IRSC-SA, we proposed a framework of DE for throughput analysis by tracking more variables and calculating the posterior probabilities based on Bayes' formula. Taking different types of users and slots into consideration, the proposed DE ideally suits the structure of IRSC-SA and evaluates the performance more exactly.

The remainder of this paper is organized as follows. In Section 2, we introduce the model of conventional CSA and the proposed IRSC-SA including the a new frame structure, user initialization, presentation by tanner graph and the definition of achievable throughput. In Section 3, we analyze the throughput of the proposed scheme and modify the conventional DE method to evaluate IRSC-SA. Based on that, the numerical and Monte-Carlo simulation results are presented in Section 4 to illustrate the performance of our proposed scheme. Finally, we conclude the paper in Section 5.

In this paper, the notations are presented as follows. Vectors and matrices are represented by boldface letters. Lowercase letters with subscript i denote the i-th entry of vectors. Lowercase letters with subscript i, j denote the i-th element in the j-th row of matrices. The transpose of a matrix is denoted by a superscript T. The probability that the Event A occurs is denoted as $\Pr\{\text{Event}\{A\}\}$. The condition probability is denoted as $\Pr\{\text{Event}\{A\}|\text{Event}\{B\}\}$

2 System model

2.1 Coded slotted ALOHA for mMTC

We consider a synchronized contention-based access system with M users. A frame consisting of N slots is assumed as a contention period, where the length of a slot corresponds to the period of a packet. Users may become active with a relatively small probability ε within a frame, and then transmits replicas of its packet on several slots in the frame. Define M_a as the number of active user in a frame. Each user transmits its burst (i.e., packet) for l times with probability Λ_l within a frame, where $1 \leqslant l \leqslant L$. Figure 1 shows the transmission process of CSA by a tanner graph.

As shown in Figure 1, the transmission process is formulated as a Tanner graph, where users and slots are represented by BNs and SNs, respectively. An edge that connects a BN and an SN represents one burst transmission. As shown in Figure 1, bursts that belongs to different users may collide on the same slot, resulting in interferences among users. To describe the slot utilization in a frame with M_a users, we define an indicator matrix $\boldsymbol{S}^{[M_a,N]} = [\boldsymbol{s}_1, \boldsymbol{s}_2, \ldots, \boldsymbol{s}_{M_a}]^{\mathrm{T}}$, where $\boldsymbol{s}_i = [s_{i,1}, s_{i,2}, \ldots, s_{i,N}]^{\mathrm{T}} \in [0,1]^N$ $(1 \leqslant i \leqslant M_a)$ indicates the transmission status of i-th user. And $s_{i,j} = 1$ indicates the burst of i-th user is transmitted on j-th slot of the considered frame and vice versa. The $\boldsymbol{S}^{[4,5]}$ that corresponds to Figure 1 is given by

$$\boldsymbol{S}^{[4,5]} = \begin{pmatrix} 0 & 1 & 0 & 1 & 1 \\ 0 & 1 & 0 & 1 & 0 \\ 1 & 0 & 0 & 0 & 1 \\ 0 & 1 & 0 & 0 & 0 \end{pmatrix}. \tag{1}$$

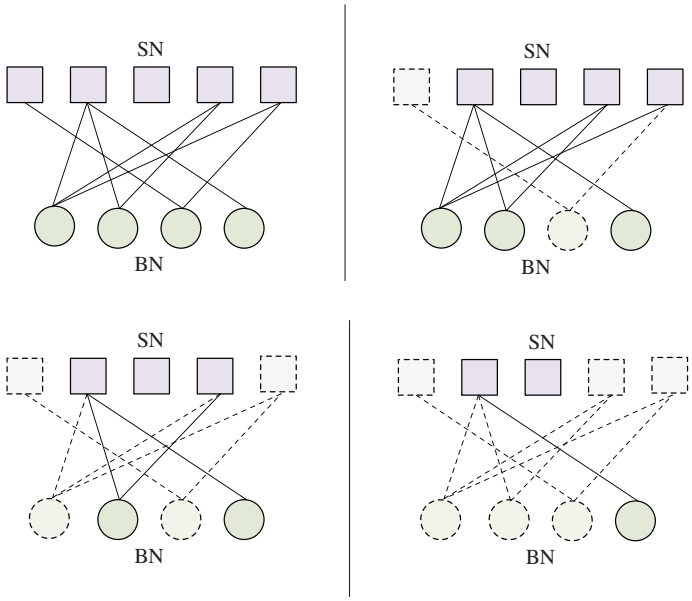

Figure 1 (Color online) An illustration of the Tanner graph of CSA and SIC.

When all the users finish the transmissions in a frame, the receiver applies SIC to separate the bursts and recovers the transmitting information [17]. A burst that is received without collision is called a clean burst and can be correctly decoded. Replicas of that recovered burst are canceled from the slots where they are located. When all interfering bursts are canceled from one slot, the only remaining burst can be then decoded. The SIC process continues until all source packets are recovered, or no clean burst exists in a frame [17]. Figure 1 shows the execution of the SIC algorithm on a graph.

2.2 Proposed IRSC-SA

In IRSC-SA, a super-frame is defined as a contention period, which consists of $M_f = L + d - 1$ frames where d is the spatial coupling length. Each frame is further divided into N slots. In IRSC-SA, there are M users in the system, each user may become active with a relatively small probability ε within a frame. Define M_a as the total number of active users in the super-frame. We note that each user transmits at most one burst packet (and its replicas) in a super-frame, and each packet transmission takes one slot. When a user become active, it transmits replicas of its packet on several slots of the current frame as well as the following $d-1$ frames. That is to say, if a user initiates packet transmission in frame-j ($1 \leqslant j \leqslant L$), it then respectively and independently selects d_k slots in frame-k ($j \leqslant k \leqslant j + d - 1$) according to the local degree distribution $\Lambda(x)$, and transmits its replicas on these slots separately. New transmissions are not allowed in the last $d - 1$ frames of a super-frame. After receiving a super-frame, SIC is applied at the receiver to recover the packets [31].

We illustrate the proposed IRSC-SA protocol with Figure 2, where BNs and SNs are grouped into different classes, respectively.

We define the BNs that initialize transmissions in i-th frame as type-i BNs and the corresponding users as type-i users. Similarly, we define SNs that belong to j-th frame as type-j SNs and the corresponding slots as type-j slots. Let δ_j be the number of BN types which connect to type-j SNs, which is represented by

$$\delta_j = \begin{cases} j, & 1 \leqslant j \leqslant d-1, \\ d, & d \leqslant j \leqslant L+d-1. \end{cases} \tag{2}$$

Then we denote $\mathcal{N}_j^s = \{j - \delta_j + 1, j - \delta_j + 2, \ldots, \min(j, L)\}$, $1 \leqslant j \leqslant M_f$, as the group of the indexes of these BN types. Similarly, we denote $\mathcal{N}_i^b = \{i, i+1, \ldots, i+d-1\}$, $1 \leqslant i \leqslant L$, as the group of the indexes of the SN types that connect to type-i BNs.

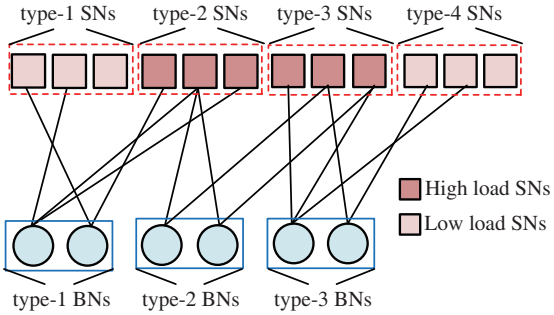

Figure 2 (Color online) Tanner graph of IRSC-SA with $L = 3$, $d = 2$, $N = 3$, $\epsilon M = 2$, and $\Lambda(x) = \frac{5}{6}x + \frac{1}{6}x^2$. The normalized average offered traffic $G = \frac{\varepsilon ML}{M_f N} = \frac{1}{2}$.

We can define a status indicator matrix to illustrate the above transmission process for IRSC-SA as $\boldsymbol{S}^{[M_a, N\times(L+d-1)]} = [\boldsymbol{s}_1, \boldsymbol{s}_2, \ldots, \boldsymbol{s}_M]^{\mathrm{T}}$. Without loss of generality, we assume the users are sorted according to the order of activation, and an example of $\boldsymbol{S}^{[M_a, N\times(L+d-1)]}$ is given in (3) with $N = 3$, $d = 3$ and $\epsilon M = 2$, where $\mathbf{0}^{[2,3]}$ is a null matrix. A 2×3 matrix describes the burst transmission of 2 users in a frame which consists of 3 slots.

$$\boldsymbol{S}^{[20,3\times10]} = \begin{bmatrix} \begin{pmatrix}1&0&0\\0&1&1\end{pmatrix} & \begin{pmatrix}0&0&1\\0&1&0\end{pmatrix} & \begin{pmatrix}0&0&1\\1&0&0\end{pmatrix} & \mathbf{0}^{[2,3]} & \cdots & \mathbf{0}^{[2,3]} & \mathbf{0}^{[2,3]} & \mathbf{0}^{[2,3]} \\ \mathbf{0}^{[2,3]} & \begin{pmatrix}1&0&0\\0&0&1\end{pmatrix} & \begin{pmatrix}0&0&1\\1&1&0\end{pmatrix} & \begin{pmatrix}0&1&1\\1&0&0\end{pmatrix} & \cdots & \mathbf{0}^{[2,3]} & \mathbf{0}^{[2,3]} & \mathbf{0}^{[2,3]} \\ \cdots & \cdots & \cdots & \cdots & \cdots & \cdots & \cdots & \cdots \\ \mathbf{0}^{[2,3]} & \mathbf{0}^{[2,3]} & \mathbf{0}^{[2,3]} & \mathbf{0}^{[2,3]} & \cdots & \begin{pmatrix}1&0&1\\0&1&0\end{pmatrix} & \begin{pmatrix}0&1&0\\1&0&0\end{pmatrix} & \mathbf{0}^{[2,3]} \\ \mathbf{0}^{[2,3]} & \mathbf{0}^{[2,3]} & \mathbf{0}^{[2,3]} & \mathbf{0}^{[2,3]} & \cdots & \begin{pmatrix}1&0&0\\0&0&1\end{pmatrix} & \begin{pmatrix}0&0&1\\0&1&0\end{pmatrix} & \begin{pmatrix}1&1&0\\1&0&0\end{pmatrix} \end{bmatrix}. \tag{3}$$

The total degree d_{sum} of a burst node is defined as the total number of burst repetition of the corresponding user. For example, $d_{\mathrm{sum}} = 3$ for the first burst node indicated in (3) and $d_{\mathrm{sum}} = 4$ for the second burst node. Then, we define $d_{\mathrm{sum,ave}}$ as the expectation value of d_{sum}.

The spatially-coupled structure further facilitates the propagation of this benefit to the neighboring BN types via SIC. It is apparent that the average number of packets transmitted in frame-k_s ($1 \leqslant k_s \leqslant d-1$) and frame-$k_b$ ($L+1 \leqslant k_b \leqslant L+d-1$) is smaller and these packets are less prone to packet erasures during transmissions. Hence the packets therein have higher probabilities to be recovered. Then source packets from type-k_s and type-k_b users are canceled to facilitate the recovery in the neighboring frames. With the spatially-coupled structure, this benefit is further propagated to the entire super-frame via SIC detection.

The throughput of IRSC-SA is evaluated as follows. Define $G^{\dagger} = (\varepsilon M)/N$ as the normalized number of initialized users in each of the first L frames, the normalized average offered traffic of a super-frame G is given by

$$G = \frac{G^{\dagger}L}{M_f} = \frac{\varepsilon ML}{NM_f}. \tag{4}$$

Define the number of packets which are correctly recovered after SIC as m, hence the system throughput T is calculated as $T = m/(M_f N)$.

3 Throughput analysis

In this section, we develop a novel DE method to analyze the throughput of IRSC-SA, and compare the proposed DE with the existing DEs [6–10, 12].

3.1 Degree distribution

Degree distribution determines the transmission pattern of each user and effects the collision situation in each slots. The degree of a BN is l represents that this burst is replicated l times. The degree of a SN is l represent that l burst replicas are transmitted within this slot. The node-perspective degree distributions of BNs and SNs can be respectively defined by the polynomials

$$\Lambda(x) \triangleq \sum_l \Lambda_l x^l, \tag{5}$$

$$\Psi^{(j)}(x) \triangleq \sum_l \Psi_l^{(j)} x^l, \tag{6}$$

where Λ_l is the probability that a BN has degree l in a frame, and $\Psi_l^{(j)}$ is the probability that a type-j SN has degree l. Obviously, the average local BN degree and the average degree of type-j SNs in a frame are given by

$$\Lambda'(1) = \sum_l l\Lambda_l, \tag{7}$$

$$\Psi^{(j)'}(1) = \sum_l l\Psi_l^{(j)}. \tag{8}$$

The edge-perspective degree distribution can be derived based on the node degree distributions. Denote λ_l as the probability that an edge is connected to a BN in the same frame with degree l, and $\rho_l^{(j)}$ as the probability that an edge is connected to a type-j SN with degree l. λ_l and $\rho_l^{(j)}$ can be derived as

$$\lambda_l = \frac{\Lambda_l l}{\sum_l \Lambda_l l}, \tag{9}$$

$$\rho_l^{(j)} = \frac{\Psi_l^{(j)} l}{\sum_l \Psi_l^{(j)} l}. \tag{10}$$

Therefore, the edge-perspective degree distributions are given as follows [15]:

$$\lambda(x) \triangleq \sum_l \lambda_l x^{l-1} = \frac{\Lambda'(x)}{\Lambda'(1)}, \tag{11}$$

$$\rho^{(j)}(x) \triangleq \sum_l \rho_l^{(j)} x^{l-1} = \frac{\Psi^{(j)'}(x)}{\Psi^{(j)'}(1)}. \tag{12}$$

When $N \to \infty$, the number of users that transmit within a slot follows the Poisson distribution. In IRSC-SA, since the normalized traffic on frame-j is $G^{(j)} = \delta_j \Lambda'(1) G^\dagger$, $\Psi^{(j)}(x)$ and $\rho^{(j)}(x)$ are respectively given by [31]

$$\Psi^{(j)}(x) = \exp(-G^\dagger \delta_j \Lambda'(1)(1-x)), \tag{13}$$

$$\rho^{(j)}(x) = \frac{\Psi^{(j)}(x)}{\Psi^{(j)'}(1)} = \exp(-G^\dagger \delta_j \Lambda'(1)(1-x)), \tag{14}$$

where $\Lambda'(1)$ denotes the derivative of $\Lambda(x)$ at $x = 1$.

3.2 Motivations

DE techniques have been developed to analyze the throughputs of various graph-based SA schemes [15, 22–25, 31]. Conventional DE assumes that all messages, from the same SN type towards different BN types, hold the same erasure probability. Conventional DE also assumes that the erasure probability of the messages, from different BN types towards the same SN types, is given by averaging the erasure probabilities of the messages from all BNs which may connect to this SN type. It is insufficient to apply the conventional DE when there are different classes/types of slot nodes and burst nodes, yielding different erasure probabilities in the graph-based SA scheme.

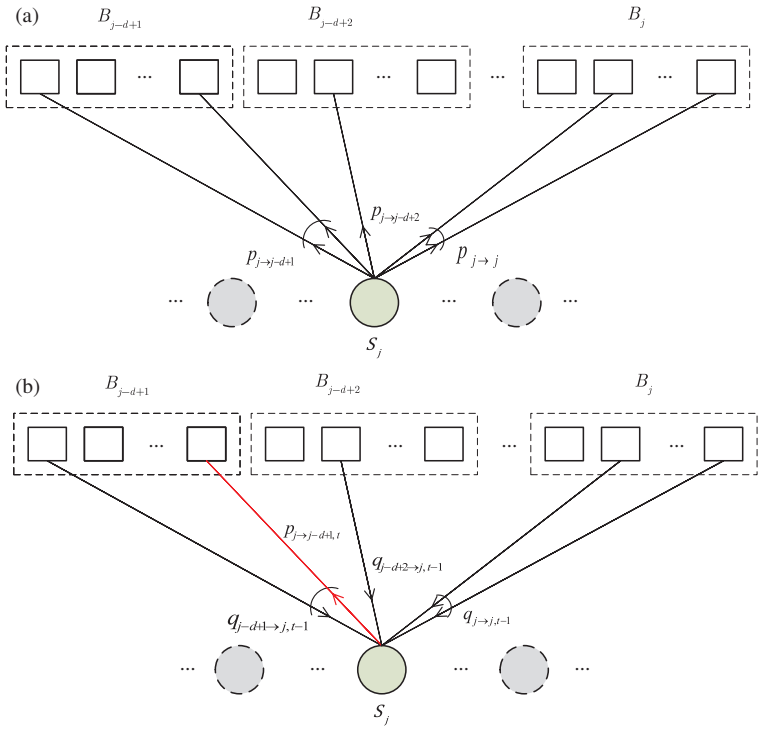

Figure 3 (Color online) The graph connections of a type-j SN indicate the message passing. (a) The erasure probability from a type-j SN towards different types of BNs; (b) the erasure probability from a BN towards a type-j SN.

One major difference between the proposed DE and the conventional DE is that the former tracks all erasure probabilities for different BN types and SN types. It suffices to use the conventional DE only to analyze the throughput of existing graph-based ALOHA schemes, where SNs and BNs are treated equivalently in terms of packet erasure probability. When BNs have varying priorities [22], different error protection properties [23,24], or different collision situations [31], DE has been modified by differentiating among different BN types and treating the erasure probability at an SN as the arithmetic average of the erasure probabilities that result from the corresponding BNs. However, these DEs assume that the edges from an SN type towards different BN types have the same erasure probability. To address this drawback, the DE in [25] divides the edge from SNs to BNs into two types. However, none of the methods above fits for the proposed IRSC-SA scheme because of the various erasure probabilities that different SNs and BNs have. To address this issue, our proposed DE tracks all $p_{j\to i}$ and $q_{i\to j}$ for all i and j, while conventional DEs ignore the differences among edges from different SN classes to different BN classes.

3.3 The proposed DE

The threshold G^* is defined as the supremum offered traffic G such that, in the asymptotic setting, i.e., the length N of frame goes to infinity, the normalized throughput T equals to G. For values of G below the threshold G*, the iterative SIC receiving will succeed with probability close to 1, and all the packets are able to be recovered. Above the threshold G*, the receiving procedure will fail with a probability bounded away from 0. We now evaluate the threshold G^* of IRSC-SA by analyzing the probabilities that source packets can be recovered. During SIC, we denote $p_{j\to i}$ as the average probability that an edge from a type-j SN to a type-i BN is not revealed, and denote $q_{i\to j}$ as the probability that an edge from a type-i BN to a type-j SN is not revealed. The graph connectivity of type-j SNs is shown in Figure 3(a) and (b) to indicate the message passing in the DE more clearly.

3.3.1 *Erasure probability from SNs to BNs*

To begin with, we define a vector $\boldsymbol{N}_j = [\ldots, n_\imath, \ldots]$ where $\imath \in \mathcal{N}_j^s$, to represent the connection status of a type-j SN, where $n_\imath \geqslant 0$ is the number of edges connecting that SN and type-$\imath$ BNs. We analyze

the erasure probability carried by an edge which connects a type-j SN to a type-i BN. Furthermore, the connection status of the type-j SN connected by the known edge is given by the vector $\boldsymbol{N}_{j|i} = [n_{j-\delta_j+1}, n_{j-\delta_j+2}, \ldots, n_i, \ldots, n_j]$, where $n_i \geqslant 1$ and $n_\imath \geqslant 0$ ($\imath \in \mathcal{N}_j^s, \imath \neq i$). Assuming that the total degree of this type-j SN is h, we denote $P_h(\boldsymbol{N}_{j|i})$ as the probability that with $n_i \geqslant 1$, the numbers of edges connecting type-$\imath$ ($\imath \in \mathcal{N}_j^s$) BNs and the type-$j$ SN is $\boldsymbol{N}_{j|i}$. Hence, $p_{j\to i}$ is calculated according to Proposition 1.

Proposition 1. The average probability $p_{j\to i,t}$ that an edge from a type-j SN to a type-i BN is not revealed after t-th iteration in SIC, is calculated as

$$\begin{aligned} p_{j\to i,t} = 1 - \sum_{h=1}^{\infty} \rho_h^{(j)} \sum_{n_{j-\delta_j+1}+\cdots+n_j=h-1} & P_h(\boldsymbol{N}_{j|i}) \\ \times (1-q_{j-\delta_j+1\to j,t})^{n_{j-\delta_j+1}} \cdots (1-q_{i\to j,t})^{n_i-1} \cdots (1-q_{j\to j,t})^{n_j}, & \end{aligned} \tag{15}$$

where $P_h(\boldsymbol{N}_{j|i})$ is given by

$$\begin{aligned} P_h(\boldsymbol{N}_{j|i}) = & \frac{1}{{\delta_j}^h - (\delta_j-1)^h} \times \binom{n_i}{h-n_{j-\delta_j+1}-\cdots-n_{i-1}} \\ & \times \prod_{\substack{\imath=j-\delta_j+1 \\ \imath\neq i}}^{j} \binom{n_\imath}{h-1-\sum_{u=j-\delta_j+1}^{\imath-1} n_u}. \end{aligned} \tag{16}$$

Proof. It is sufficient to consider an arbitrary edge $\mathcal{E}_{i\leftrightarrow j}$ connecting a type-j SN and a type-i BN which are referred to as $\mathcal{S}_j$ and $\mathcal{B}_i$, respectively. In what follows we derive $p_{j\to i,t}$ by traversing the probability space of all possible connection statuses of $\mathcal{S}_j$ and then applying the sum-product algorithm.

Assume that $\mathcal{S}_j$ has degree h. It is known that $\mathcal{S}_j$ connects to h edges and at least one connection corresponds to $\mathcal{B}_i$, thus the rest $h-1$ edges are less likely to be connected to $\mathcal{B}_i$. Hence, we can use $\boldsymbol{N}_{j|i}$ to describe the connection status of $\mathcal{S}_j$, and use $P_h(\boldsymbol{N}_{j|i})$ to describe the conditional occurrence probability of $\boldsymbol{N}_{j|i}$, under the condition that $n_i \geqslant 1$ (due to the existence of $\mathcal{E}_{i\leftrightarrow j}$). This motivates us to apply the Bayes' theorem in calculating $P_h(\boldsymbol{N}_{j|i})$ as follows. Let $r_\imath$ denote the unconditional probability that an arbitrary edge that connects to $\mathcal{S}_j$ comes from a type-$\imath$ BN. We define Event$\{\boldsymbol{N}_j\}$ as the event that the connection status of the type-j SN is according to $\boldsymbol{N}_j$. Besides, we define Event$\{\mathcal{E}_{i\leftrightarrow j}\}$ as the event that there exists an edge between the type-j SN and a type-i BN. Then $P_h(\boldsymbol{N}_{j|i})$ is calculated based on Bayes' formula as in (17).

$$\begin{aligned} P_h(\boldsymbol{N}_{j|i}) = & \ \Pr\{\text{Event}\{\boldsymbol{N}_j\}|\text{Event}\{\mathcal{E}_{i\leftrightarrow j}\}\} = \frac{\Pr\{\text{Event}\{\boldsymbol{N}_j\} \ \& \ \text{Event}\{\mathcal{E}_{i\leftrightarrow j}\}\}}{\Pr\{\text{Event}\{\mathcal{E}_{i\leftrightarrow j}\}\}}, \\ = & \left(\binom{n_{j-\delta_j+1}}{h-1}(r_{j-\delta_j+1})^{n_{j-\delta_j+1}} \cdots \binom{n_i}{h-n_{j-\delta_j+1}-\cdots-n_{i-1}}(r_i)^{n_i} \cdots \binom{n_j}{h-1-n_{j-\delta_j+1}-\cdots-n_{j-1}}(r_j)^{n_j}\right) \\ & /(1-(1-r_i)^h), \\ = & \frac{\prod_{\substack{\imath=j-\delta_j+1 \\ \imath\neq i}}^{j} \binom{n_\imath}{h-1-\sum_{u=j-\delta_j+1}^{\imath-1} n_u} (r_\imath)^{n_\imath} \times \binom{n_i}{h-n_{j-\delta_j+1}-\cdots-n_{i-1}}(r_i)^{n_i}}{1-(1-r_i)^h}. \end{aligned} \tag{17}$$

Since all BN types in $\mathcal{N}_j^s$ are equally accessible to $\mathcal{S}_j$, we have $r_\imath = 1/\delta_j$ ($\imath \in \mathcal{N}_j^s$). Substitute $r_\imath$ into (17) and we get (16).

Now we are ready to derive (15). Given $\boldsymbol{N}_{j|i}$, $n_\imath$ represents the number of edges that connect $\mathcal{S}_j$ and type-$\imath$ ($\imath \in \mathcal{N}_j^s \backslash i$) BNs, and $(1-q_{\imath\to j,t})^{n_\imath}$ represents the probability that all edges from type-$\imath$ BNs are revealed to $\mathcal{S}_j$ after t-th SIC iteration. Besides, $(1-q_{i\to j,t})^{n_i-1}$ represents the probability that the other n_i-1 edges (except $\mathcal{E}_{i\leftrightarrow j}$) from type-$i$ BNs are revealed to $\mathcal{S}_j$. We note that $p_{j\to i,t}$ should be calculated according to the extrinsic information of the edges (except $\mathcal{E}_{i\leftrightarrow j}$) that are connected to $\mathcal{S}_j$ in the last SIC

iteration. Hence, $\mathcal{E}_{i\leftrightarrow j}$ is revealed only when all the other edges are revealed to $\mathcal{S}_j$, and this probability is given by multiplying $(1-q_{i\to j,t})^{n_i-1}$ with $(1-q_{\imath\to j,t})^{n_\imath}$ for all $\imath\in\mathcal{N}_j^s\backslash i$. Averaging this probability over all possible $\boldsymbol{N}_{j|i}$ and h, we get $1-p_{j\to i,t}$ as in (15).

3.3.2 *Erasure probability from BNs to SNs*

Similar to $\boldsymbol{N}_{j|i}$, we define a vector $\boldsymbol{M}_{i|j}=[\ldots,m_\jmath,\ldots]=[m_i,m_{i+1},\ldots,m_{j-1},m_{j+1},\ldots,m_{i+d-1}]$ with $\jmath\in\mathcal{N}_i^b\backslash j$, where $m_\jmath\leqslant\max_{\Lambda_l\neq 0}(l)$ and $m_\jmath$ denotes the number of edges that connect type-$\jmath$ SNs and $\mathcal{B}_i$. $P(\boldsymbol{M}_{i|j})$ denotes the probability that the numbers of edges that connect type-$\jmath$ ($\jmath\in\mathcal{N}_i^b\backslash j$) SNs and $\mathcal{B}_i$ are according to $\boldsymbol{M}_{i|j}$. The erasure probability from BNs to SNs is calculated in Proposition 2.

Proposition 2. The average probability $q_{i\to j,t}$ that an edge from a type-i BN to a type-j SN is not revealed after t-th iteration in SIC, is calculated as

$$q_{i\to j,t}=\sum_l \lambda_l\left(p_{j\to i,t-1}\right)^{l-1}\times\sum_{\boldsymbol{M}_{i|j}}\left\{P(\boldsymbol{M}_{i|j})\prod_{\jmath\in\mathcal{N}_i^b\backslash j}\left(p_{\jmath\to i,t-1}\right)^{m_\jmath}\right\},\tag{18}$$

where $P(\boldsymbol{M}_{i|j})$ is given by

$$P(\boldsymbol{M}_{i|j})=\prod_{\jmath\in\mathcal{N}_i^b\backslash j}\Lambda_{m_\jmath}.\tag{19}$$

Proof. Note that $q_{i\to j,t}$ equals the probability that all edges (except $\mathcal{E}_{i\leftrightarrow j}$) that connect to $\mathcal{B}_i$ are unknown after iteration $t-1$. Since the transmissions in different frames are independent, the number of edges that connect type-$\jmath$ ($\jmath\in\mathcal{N}_i^b\backslash j$) SNs to $\mathcal{B}_i$ only depends on $\Lambda_{m_\jmath}$. Therefore we obtain $P(\boldsymbol{M}_{i|j})$ in (19).

To calculate $q_{i\to j,t}$, we first consider the edges that connect type-j SNs and type-i BNs. The number of edges that connect to $\mathcal{B}_i$ is λ_l, thus the probability that all these edges are unknown to $\mathcal{B}_i$ is $\lambda_l(p_{j\to i,t-1})^{l-1}$. Then we consider the edges from type-$\jmath$ SNs to $\mathcal{B}_i$ where $\jmath\in\mathcal{N}_i^b\backslash j$. We consider all possible realizations of $\boldsymbol{M}_{i|j}$ according to (19), and perform weighted sum of all erasure probabilities $(p_{\jmath\to i,t-1})^{m_\jmath}$, $\jmath\in\mathcal{N}_i^b\backslash j$. Aggregating the results above, we get (18).

By initializing $p_{j\to i,0}$ and $q_{i\to j,0}$ as 1, the average probability that an edge carries an erasure message can be calculated by incorporating (18) into (15). We calculate $p_{j\to i,t}$ and $q_{i\to j,t}$ iteratively until they converge when $i\to\infty$. By iteratively updating (15) and (18), we can calculate G^* [15].

3.4 Comparison between the proposed DE and conventional DE

Our proposed DE considers the following two improvements in order to fit for the IRSC-SA scheme:

(i) IRSC-SA consists of M_f non-equivalent SN types as well as L non-equivalent BN types. All edge types between different BN types and/or SN types are tracked in DE to precisely represent the SIC process.

(ii) Consider a type-j SN with degree h that connects to various BN types. The erasure probability of a specific edge that connects this SN to one BN, e.g. a type-i BN, is calculated according to the probabilities on the other $h-1$ edges, which are less likely to come from type-i BNs according to Bayesian theorem. This prior knowledge is exploited in the proposed DE since different BN types correspond to different packet erasure probabilities due to spatial coupling. Otherwise, this prior knowledge would have resulted underestimation of the asymptotic system throughput.

As mentioned earlier, each SN may connect to h BNs from at most d types of BNs in IRSC-SA. In the proposed DE, multiple variables $p_{j\to j-\delta_j+1},\ldots,p_{j\to j}$ are defined to represent the erasure probability from a type-j SN towards type-$(j-\delta_j+1)$ to type-j BNs, and $q_{j-\delta_j+1\to j},\ldots,q_{j\to j}$ are defined to represent the erasure probability from type-$(j-\delta_j+1)$ to type-j BNs towards a type-j SN.

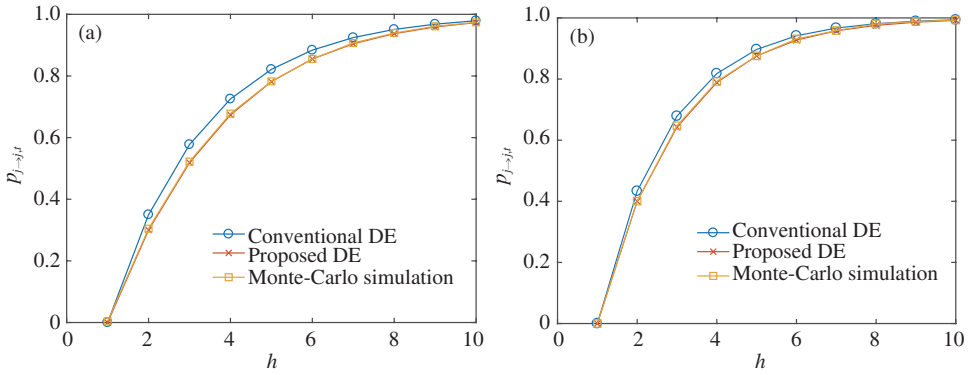

Figure 4 (Color online) Comparisons between the $p_{j\to j,t}$ derived by the proposed DE and the conventional DE. (a) $d=2$, $q_{j-1\to j,t}=0.2$, $q_{j\to j,t}=0.5$; (b) $d=3$, $q_{j-2\to j,t}=0.2$, $q_{j-1\to j,t}=0.5$, $q_{j\to j,t}=0.6$.

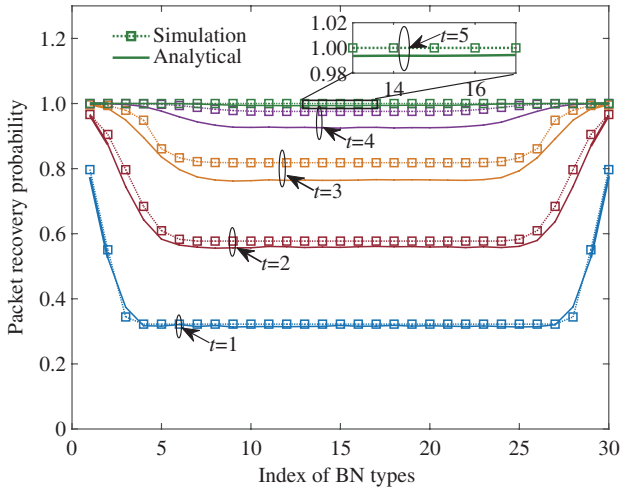

Figure 5 (Color online) The comparison of the packet recovery probabilities of different BN types during SIC iterations.

To show that conducting aggregation or arithmetic average may lose the accuracy in estimating the iterative detection threshold, we compare the erase probabilities from type-j SNs to type-j BNs derived by the proposed DE and the conventional DE respectively.

We consider two cases where $d=2$ and $d=3$ in Figure 4. For each case, we initiate the $q_{i\to j,t}$ $(i=j-d+1,\ldots,j)$ and $q'_{i\to j,t}$ $(i=j-d+1,\ldots,j)$ with the same values in both DE methods, and compare the erasure probabilities after one iteration, i.e., $p_{j\to j,t+1}$ and $p'_{j,t+1}$, derived by (15) and (18), respectively. The Monte-Carlo simulations are conducted by first randomly generating the edges between type-$(j-d-1)$ to type-j users and type-j slots (according to the SC-SA protocol in [31], since the conventional DE cannot be applied to IRSC-SA), then randomly canceling $1-q_{i\to j}$ of the edges as if they have been canceled by SIC in previous iterations, and then calculating the proportion of the edges which can be recovered by type-j SNs with SIC receiver in this iteration. 10000 slots are assumed in a type-j SNs.

4 Simulations

In this section, we present analytical and simulation results of IRSC-SA, SC-SA [31] and CRDSA [15]. To evaluate the performance of IRSC-SA, we use a $\Lambda(x)$ that achieves an optimal throughput [33]. We consider the maximum allowed local degree to be 2, i.e., $\Lambda_l=0, l\geqslant 3$, and we use $\Lambda(x)=0.9x+0.1x^2$ in IRSC-SA.

Figure 5 depicts the packet recovery probabilities of different BN types during SIC iterations with

Table 1 Thresholds of different access schemes

G^*	$d=2$	$d=3$	$d=4$
IRSC-SA	0.6138	0.9367	0.9688
SC-SA	0.5	0.9078	0.9585
CRDSA	0.5	0.8184	0.7722

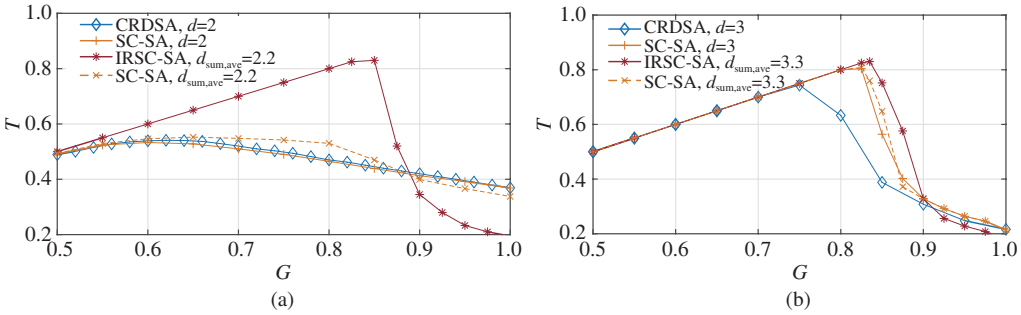

Figure 6 (Color online) Throughputs of CRDSA with $N = 400$, SC-SA with $N = 400$, and IRSC-SA with $\Lambda(x) = 0.9x + 0.1x^2$ and $N = 400$, $L = 40$. (a) $d = 2$; (b) $d = 3$.

$d = 4$, $L = 30$, $N = 1500$ and $G = 0.5$. We present both analytical and simulation results for 1 to 5 SIC iterations, where the analytical results are obtained by first iteratively calculating (15) and (18), and then average $q_{i\to j,t}, j \in \mathcal{N}_j^s$. It can be observed that, thanks to spatial coupling, packets from type-i BNs, where $1 \leqslant i \leqslant d-1$ or $L-d+2 \leqslant i \leqslant L$, have higher probabilities to be recovered. This benefit propagates through adjacent frames and improves the overall performance.

In Table 1, we derive the thresholds G^* of IRSC-SA, SC-SA and CRDSA. It is shown that the thresholds of IRSC-SA are higher than SC-SA, indicating that higher throughput can be achieved by IRSC-SA. Note that, the thresholds of IRSC-SA and SC-SA increase with larger d, while this improvement is not observed in CRDSA. This is because in IRSC-SA and SC-SA schemes, the collision probabilities in type-j frames ($1 \leqslant j \leqslant d-1$ or $L \leqslant j \leqslant L+d-1$) are smaller which improves the overall performance, hence they have lower erasure probabilities comparing to CRDSA.

Figure 6 shows the throughput performance of the proposed IRSC-SA scheme with $d = 2$ and 3. The average degree per user $d_{\text{sum,ave}}$ in IRSC-SA is $d_{\text{sum,ave}} = 2.2$ and 3.3, respectively. We also show the throughput performance of SC-SA and CRDSA. We ensure that SC-SA has the same $d_{\text{sum,ave}}$ as IRSC-SA for fair comparisons. In Figure 6(a), we consider an SC-SA scheme where 80% of users send packets with $d = 2$ and 20% of users send packets with $d = 3$, resulting in $d_{\text{sum,ave}} = 2.2$. Similarly, in Figure 6(b), 70% of users send packets with $d = 3$ and 30% of users send packets with $d = 4$, resulting in $d_{\text{sum,ave}} = 3.3$ in SC-SA. As shown in Figure 6, IRSC-SA achieves higher throughput compared to SC-SA and CRDSA, which is consistent with the threshold results in Table 1.

Figure 7 compares the achievable capacity between IRSC-SA and SC-SA schemes in additive white Gaussian noise channels with $d = 3$ and the same total transmit power P_0 per user. The achievable capacity per user is calculated with $\log_2(1 + \frac{P_0}{d_{\text{sum}} N_0})$, where d_{sum} is the total degree per user and N_0 is the noise variance. It is shown that IRSC-SA achieves slightly higher capacity than SC-SA. In IRSC-SA, the user with a higher d_{sum} has a higher probability to be recovered and hence contributes more to the throughput. However, due to the equal power constraint per user, each of these replicas is sent with lower energy and hence smaller data load, which reduces the gain in capacity compared with SC-SA. Nevertheless, we note that enhancing system throughput is key to 5G massive sporadic transmissions, and the proposed IRSC-SA achieves significantly improved system packet throughput compared with SC-SA, as discussed in this section.

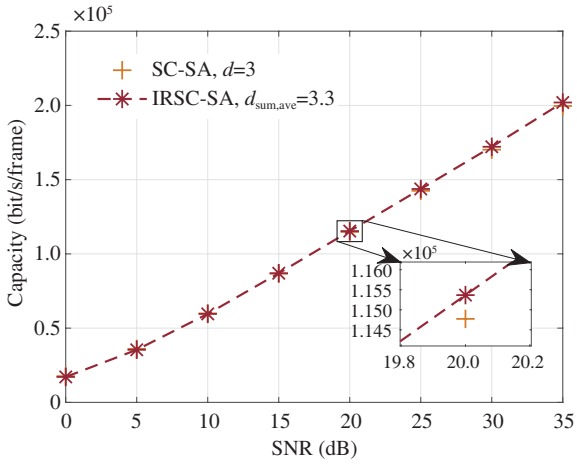

Figure 7 (Color online) Capacities of IRSC-SA and SC-SA with same transmission power per user.

5 Conclusion

In this paper, we have proposed a new contention-based access scheme by integrating spatial coupling with irregular repetition. We have designed a novel DE to analyze the proposed scheme by taking different user types and slot types into consideration, which can accurately track the packet erasure probability. Analysis and simulation results showed that the proposed scheme achieves better threshold and higher throughput performance compared to the conventional schemes.

Acknowledgements This work was partially supported by Beijing Natural Science Foundation (Grant No. L182038), Chinese Ministry of Education-China Mobile Communication Corporation Research Fund (Grant No. MCM20170101), China National S&T Major Project (Grant No. 2017ZX03001017), National Natural Science Foundation of China (Grant No. 61871032), Beijing Major Science and Technology Projects (Grant No. D171100006317001), Ericsson company, and 111 Project of China (Grant No. B14010).

References

1 Bockelmann C, Pratas N, Nikopour H, et al. Massive machine-type communications in 5G: physical and MAC-layer solutions. IEEE Commun Mag, 2016, 54: 59–65
2 3GPP. Study on Scenarios and Requirements for Next Generation Access Technologies. TR 38.913. 2018. https://www.3gpp.org/ftp/specs/archive/38_series/38.913/
3 Saad W, Bennis M, Chen M Z. A vision of 6G wireless systems: applications trends technologies and open research problems. 2019. arXiv: 1902.10265
4 Tariq F, Khandaker M, Wong K, et al. A speculative study on 6G. 2019. arXiv: 1902.06700
5 Wu J, Fan P. A survey on high mobility wireless communications: challenges, opportunities and solutions. IEEE Access, 2016, 4: 450–476
6 Saito Y, Kishiyama Y, Benjebbour A, et al. Non-orthogonal multiple access (NOMA) for cellular future radio access. In: Proceedings of IEEE 77th Vehicular Technology Conference, Dresden, 2013. 1–5
7 Yuan Y, Yuan Z, Yu G, et al. Non-orthogonal transmission technology in LTE evolution. IEEE Commun Mag, 2016, 54: 68–74
8 Taherzadeh M, Nikopour H, Bayesteh A, et al. SCMA codebook design. In: Proceedings of IEEE Vehicular Technology Conference, 2014. 1–5
9 Au K, Zhang L, Nikopour H, et al. Uplink contention based SCMA for 5G radio access. In: Proceedings of IEEE Globecom Workshops (GC Wkshps), 2014. 900–905
10 3GPP. Study on Non-Orthogonal Multiple Access (NOMA) for NR. TR 38.913. 2018. https://www.3gpp.org/ftp/specs/archive/38_series/38.812/
11 Zhang Z, Wang X, Zhang Y, et al. Grant-free rateless multiple access: a novel massive access scheme for internet of things. IEEE Commun Lett, 2016, 20: 2019–2022
12 Shirvanimoghaddam M, Li Y H, Vucetic B. Multiple access analog fountain codes. In: Proceedings of IEEE International Symposium on Information Theory, Honolulu, 2014. 2167–2171
13 Choudhury G, Rappaport S. Diversity ALOHA–a random access scheme for satellite communications. IEEE Trans Commun, 1983, 31: 450–457
14 Casini E, de Gaudenzi R, Herrero O R. Contention resolution diversity slotted ALOHA (CRDSA): an enhanced random

access schemefor satellite access packet networks. IEEE Trans Wirel Commun, 2007, 6: 1408–1419
15 Liva G. Graph-based analysis and optimization of contention resolution diversity slotted ALOHA. IEEE Trans Commun, 2011, 59: 477–487
16 Sun Z, Xie Y, Yuan J, et al. Coded slotted ALOHA schemes for erasure channels. In: Proceedings of IEEE International Conference on Communications (ICC), Kuala Lumpur, 2016. 1–6
17 Paolini E, Stefanovic C, Liva G, et al. Coded random access: applying codes on graphs to design random access protocols. IEEE Commun Mag, 2015, 53: 144–150
18 Jia D, Fei Z S, Xiao M, et al. Enhanced frameless slotted ALOHA protocol with Markov chains analysis. Sci China Inf Sci, 2018, 61: 102304
19 Cao C Z, Fei Z S, Xiao M, et al. An extended packetization-aware mapping algorithm for scalable video coding in finite-length fountain codes. Sci China Inf Sci, 2013, 56: 042311
20 Huang J X, Fei Z S, Cao C Z, et al. On-line fountain codes with unequal error protection. IEEE Commun Lett, 2017, 21: 1225–1228
21 Huang J X, Fei Z S, Cao C Z, et al. Performance analysis and improvement of online fountain codes. IEEE Trans Commun, 2018, 66: 5916–5926
22 Toni L, Frossard P. Prioritized random MAC optimization via graph-based analysis. IEEE Trans Commun, 2015, 63: 5002–5013
23 Stefanovic V, Popovski P. Coded slotted ALOHA with varying packet loss rate across users. In: Proceedings of IEEE Global Conference on Signal and Information Processing, Austin, 2013. 787–790
24 Ivanov M, Brannstrom F, Graell i Amat A, et al. Unequal error protection in coded slotted ALOHA. IEEE Wirel Commun Lett, 2016, 5: 536–539
25 Sandgren E, Graell i Amat A, Brannstrom F. On frame asynchronous coded slotted ALOHA: asymptotic, finite length, and delay analysis. IEEE Trans Commun, 2017, 65: 691–704
26 Cao C Z, Koike-Akino T, Wang Y, et al. Irregular polar coding for massive MIMO. In: Proceedings of IEEE Global Communications Conference, Singapore, 2017
27 Koike-Akino T, Cao C Z, Wang Y, et al. Irregular polar coding for complexity-constrained lightwave systems. J Lightw Technol, 2018, 36: 2248–2258
28 Koike-Akino T, Cao C Z, Wang Y. Turbo product codes with irregular polar coding for high-throughput parallel decoding in wireless OFDM transmission. In: Proceedings of IEEE International Conference on Communications (ICC), 2018. 1–7
29 Kudekar S, Richardson T J, Urbanke R L. Threshold saturation via spatial coupling: why convolutional LDPC ensembles perform so well over the BEC. IEEE Trans Inform Theor, 2011, 57: 803–834
30 Engdahl K, Lentmaier M, Zigangirov K S. On the theory of low-density convolutional codes. In: Proceedings of International Symposium on Applied Algebra, Algebraic Algorithms, and Error-Correcting Codes, 1999. 77–86
31 Liva G, Paolini E, Lentmaier M, et al. Spatially-coupled random access on graphs. In: Proceedings of IEEE International Symposium on Information Theory Proceedings (ISIT), Cambridge, 2012. 478–482
32 Richardson T J, Shokrollahi M A, Urbanke R L. Design of capacity-approaching irregular low-density parity-check codes. IEEE Trans Inform Theor, 2001, 47: 619–637
33 Narayanan K R, Pfister H D. Iterative collision resolution for slotted ALOHA: An optimal uncoordinated transmission policy. In: Proceedings of International Symposium on Turbo Codes and Iterative Information Processing (ISTC). Gothenburg, 2012. 136–139